Accepted Manuscript

Crystallization derivation of amine functionalized T_{12} polyhedral oligomeric silsesquioxane-conjugated poly(ethylene terephthalate)

Albert S. Lee, Hyeonyeol Jeon, Seung-Sock Choi, Jeyoung Park, SungYeon Hwang, Jonggeon Jegal, Dongyeop X. Oh, Byoung Chul Kim, Seung Sang Hwang

PII: S0266-3538(17)30292-0

DOI: 10.1016/j.compscitech.2017.04.015

Reference: CSTE 6745

To appear in: *Composites Science and Technology*

Received Date: 8 February 2017

Revised Date: 31 March 2017

Accepted Date: 12 April 2017

Please cite this article as: Lee AS, Jeon H, Choi S-S, Park J, Hwang S, Jegal J, Oh DX, Kim BC, Hwang SS, Crystallization derivation of amine functionalized T_{12} polyhedral oligomeric silsesquioxane-conjugated poly(ethylene terephthalate), *Composites Science and Technology* (2017), doi: 10.1016/j.compscitech.2017.04.015.

This is a PDF file of an unedited manuscript that has been accepted for publication. As a service to our customers we are providing this early version of the manuscript. The manuscript will undergo copyediting, typesetting, and review of the resulting proof before it is published in its final form. Please note that during the production process errors may be discovered which could affect the content, and all legal disclaimers that apply to the journal pertain.

ACCEPTED MANUSCRIPT

Crystallization derivation of amine functionalized T_{12} polyhedral oligomeric silsesquioxane-conjugated poly(ethylene terephthalate)

Albert S. Lee,[1+] Hyeonyeol Jeon,[2+] Seung-Sock Choi,[1+] Jeyoung Park,[2,3] SungYeon Hwang,[2,3] Jonggeon Jegal,[2] Dongyeop X. Oh,[2,3,*] Byoung Chul Kim,[4,*] Seung Sang Hwang[1,*]

[1]Materials Architecturing Research Center, Korea Institute Science and Technology (KIST), Seoul 02792, Republic of Korea.

[2]Research Center for Bio-based Chemistry, Korea Research Institute of Chemical Technology (KRICT), Ulsan 44429, Republic of Korea.

[3]Advanced Materials and Chemical Engineering, University of Science and Technology (UST), Daejeon 305-333, Republic of Korea.

[4]Division of Applied Chemical and Bio Engineering, Hanyang University, Seoul, South Korea.

[+]These authors equally contributed to this work.

*Correspondence: dongyeop@krict.re.kr (D. X. Oh) Tel.: +82-52-241-6316; Fax: +82-52-241-6349, bckim@hanyang.ac.kr (B. C. Kim) Tel.: +82-2-2290-0494; Fax: +82-2-2297-4941, sshwang@kist.re.kr (S. S. Hwang) Tel.: +82-2-958-5314; Fax: +82-2-958-5309

KEYWORDS: A. Functional composites, A. Nano composites, A. Particle-reinforced composites, B. Thermomechanical properties, B. Interphase

ACCEPTED MANUSCRIPT

ACCEPTED MANUSCRIPT

ABSTRACT

Most inorganic nucleating agents for poly(ethylene terephthalate) (PET) have limited nucleating ability due to poor compatibility with PET. Polyhedral oligomeric silsesquioxanes (POSS) is a type of cage-shaped organic/inorganic hybrid nanoparticles with three different particle sizes: octameric (T_8), decameric (T_{10}), and dodecameric (T_{12}). POSS is considered as a promising nucleating agent for PET because the inorganic moieties contribute to high thermal stability and nucleation and the organic moieties can be tethered to PET chains. In contrast to T_8 POSS, the nucleation ability of T_{12} POSS for PET has been poorly reported. In this study, our newly synthesized aminopropyl functionalized T_{12} POSS (A-POSS) is proposed as a potential nucleating agent for PET. The amine group of A-POSS is able to be chemically conjugated to PET chains, thereby giving a more homogeneous dispersion of T_{12} POSS in PET than non-functional T_{12} Phenyl POSS (N-POSS). Its PET composites gave a ~1.2 fold higher crystallization temperature and ~2.7 fold higher shear-induced crystallization rate over pristine PET. Such nucleating effects for PET is more effective than those of non-functional T_{12} POSS and the more widely studied T_8 POSS. This strategy is potentially beneficial for the high-shear melt processes of PET such as spinning and film extrusion.

ACCEPTED MANUSCRIPT

ACCEPTED MANUSCRIPT

1. Introduction

Poly(ethylene terephthalate) (PET) is a versatile commercial thermoplastic polymer [1, 2], widely seen in everyday life as plastic bottles or containers for foods or as fibrous clothing. PET is melt-processed through injection molding and extrusion blow molding to obtain desired forms such as films and fibers, exhibiting exceptional processability. However, despite these advantages, the low crystallization rate of PET leads to the post-shrinkage of products, retardation of melt process rate, consequently leading to a decrease in mechanical properties [1, 2].

To increase crystallization rate, PET is commonly copolymerized or blended with poly(butylene terephthalate) (PBT) [3, 4]. However the use of the butylated form generally compromises thermal and mechanical properties. Alternative strategies have entailed the introduction of nucleating agents to increase the crystallization rate of PET. However, organic chemical-based nucleating agents suffer from thermal degradation in PET melts as processing temperatures above the high melting point of ~250 °C [5] are often too high for organics. Inorganic nanoparticles such as nano-clay, carbon nanotubes, and nano-silica possess a high potential as nucleating agents for PET composite because they improve the mechanical and thermal properties of PET [2, 6-8]. However, the critical issue about utilizing inorganic nucleating agents is their poor dispersion in PET; its effects in increasing the crystallization rate have proved modest [2].

Polyhedral oligomeric silsesquioxane (POSS) is an organic/inorganic hybrid nanoparticle and a potential nucleating agent for PET. POSS contains a basic polyhedral Si-O nano-structured cage with a ratio of Si:O of 1:1.5. T_8, T_{10}, and T_{12} POSS have 8, 10, or 12 Si atoms located at the corner of the cages, to which 8, 10, or 12 organic groups are attached respectively (**Fig. 1a.**) [9-11]. POSS withstands the high melting temperature of PET due to the Si core, and the organic moieties of POSS can be chemically conjugated to the carboxylic acid of PET chains during melt process [12-14]. T_8 POSS has been highly reported to improve the crystallization rate of PET [10, 12, 13]. However, different types of T_8 POSS have respective disadvantages as a filler of PET. The addition of epoxy functional T_8 POSS

increases the viscosity of PET, which possibly degrades the processability [14]. The addition of open cage T_8 POSS rather retards the crystallization rate, lowering the crystallization temperature of PET during the cooling trace after melting [12]. T_{12} POSS has been poorly studied as the filler of PET. Thus, it is worth to study the effects of T_{12} POSS on PET crystallization.

In this study, the effects of T_{12} POSS and its amine functional group on the crystallization behavior of PET were investigated, where in-depth characterizations were also carried out to investigate the effects of chemical conjugation between T_{12} POSS and PET on the homogeneity and rheological properties of PET/T_{12} POSS composites.

2. Experimental

2.1. Materials

PET was provided by SK Chemicals (SKY PET BL, SK Chemical, Korea). According to the material information of SK Chemicals, its melt viscosity at 275 ºC under the shear rate of 10,000 s^{-1} is 670 poise. Phenyltrimethoxysilane (Gelest, 98%), 3-aminopropyltrimethoxysilane (Gelest, 98%), and tetrahydrofuran (J.T. Baker, HPLC grade) were vacuum distilled prior to use. K_2CO_3 (Sigma Aldrich, 99.999%) was dried at 40 ^oC under vacuum prior to use. All other solvents were used as received.

2.2 Synthesis of A-POSS and N-POSS

In our previous work, the facile high-yield synthesis of T_{12} POSS under mildly basic aqueous conditions at room temperature was reported [15, 16]. Two types of T_{12} POSS were synthesized using a modified literature procedure (**Fig. 1a**.): amine-functionalized T_{12} POSS (A-POSS) and dodecaphenyl T_{12}-phenyl POSS (non-reactive POSS; N-POSS) [15, 16]. In a typical experiment, a solution of potassium carbonate (0.04 g, 0.29 mmol) dissolved in distilled water (4.8 g, 0.27 mol) with 80 g of tetrahydrofuran (THF) was prepared. To this solution, a mixture of phenyltrimethoxysilane (11.9 g, 60 mmol) and/or either 3-aminopropyltrimethoxysilane (1.79 g, 10 mmol) was added all at once. The reaction mixture was stirred vigorously at room temperature for 72 hrs. The volatiles were rotary-evaporated under

vacuum and precipitated in freshly distilled water to obtain a white, semi-crystalline powder, which was dried under vacuum at 40 °C overnight. The obtained powders were recrystallized in a 9/1 vol/vol THF/Acetonitrile solvent mixture to yield fine crystals. (12 g, 80% yield). The main structures of amine functionalized T_{12} POSS is suggested in **Fig. 1**. The A-POSS has two amine groups on average, and the position of the amine groups in the A-POSS is irregular. Matrix-assisted laser desorption/ionization (MALDI-TOF) for N-POSS and A-POSS gave m/z 1630 (PDI = 1.08) and m/z 1550 (PDI = 1.08), respectively. A-POSS: ^{1}H NMR ($(CD_3)_2SO$) δ=0.4 (t, 2H), δ=1.3 (m, 2H), δ=2.7 (t, 2H), δ=6.5-8.0 (m, 35H). N-POSS ^{1}H NMR (THF-*d8*) δ=7.4 (t, 1H), δ=7.2 (t, 2H), δ=7.1 (d, 2H). M_n = 1,300, PDI = 1.10 (A-POSS); M_n = 1,300, PDI = 1.06 (N-POSS). In our previous report, dilute solution small-angle X-ray scattering (SAXS) and microscopic analysis for T_{12} POSS were unable to give its particle size because the size of T12 POSS is too small [16]. However, a typical size of T_{12} POSS is estimated to have 1-3 nm in consideration of the bond length of Si-O and C-C [17]. Supplementary information includes Fourier-transform infrared spectroscopy (FT-IR) data of A-POSS and N-POSS (**Fig. S1.**) [15, 16].

2.3. Characterization

X-ray photoelectron spectroscopy (XPS) studies were performed with PHI 5800 ESCA system (Physical Electronics, Chanhassen, MN, USA) at $2x10^{-10}$ torr with a monochromatic Al Kα (1486.6 eV) anode (250W, 10kV, 27mA). Onset melting temperature, glass transition temperature (T_g), and crystallization temperature were investigated on a differential scanning calorimeter (DSC) (TA Instrument DSC model Q20, New Castle, DE, USA). The specimens were heated up to 300 °C at a heating rate of 20 °C/min, held in the molten state for 5 min, then cooled down to 30 °C at a cooling rate of 10 °C/min in nitrogen atmosphere. Rheological properties were measured by an advanced rheometric expansion system (TA Instrument, New Castle, DE, USA). Parallel plate geometry with a diameter of 25 mm was employed in an oscillatory mode. The plate gap and strain level were 1 mm and 10%, respectively. To determine shear-induced crystallization time, the fully melted samples were cooled down to 220 °C, and then the time dependent dynamic storage modulus of the samples were measured

with the angular frequency (ω) of 0.5 at 220 °C. The specimen was melted at 280 °C between the parallel plates and the excess flushed-out sample during gap-setting was trimmed off. Frequency sweep measurements were conducted at 280 °C. The Si atom mapping image of PET composites surfaces were obtained using a field emission electron probe microanalyzer (FE-EPMA) (JXA-8500F, JEOL, Tokyo, Japan). MALDI-TOF MS data were obtained using a 4800 MALDI-TOF/TOF analyzer (Voyager DE STR workstation, Applied Biosystems) with dithranol and NaCl mixture as the matrix and ionization dopant, respectively. The spectra were recorded using linear ion mode irradiated under high vacuum. Wide angle X-ray scattering analysis (WAXS) was conducted with a Rigaku, ATX-G high resolution diffractometer employing Ni-filtered Cu K radiation. Dried sample films were mounted on an aluminum sample holder, and scanning angle was varied from 5 to 55^{o} at a scanning rate of 5^{o}/min. All spectra were measured at ambient temperature.

2.4. Fabrication of PET/POSS Composites

The two types of PET/T_{12} POSS composites were prepared using A-POSS or N-POSS. PET and T_{12} POSS were dried at 80 °C for 24 h and tumbled in a bag, then followed by melt-compounding in an internal mixer (Haake Rheomix-600, Leawood, KS, USA) for 5 min at 280 °C at a rotor speed of 50 rpm. The samples were cryogenically ground into fine powder, then the powder was melt-processed to films using hot pressing molding. The samples are listed in **Table 1**.

3. Results and Discussion

3.1. Conjugation of functionality between PET and POSS

The amine group of A-POSS reacts with the carboxylic acid of PET. Thus, the A-POSS was chemically conjugated to PET chains. The chemical reaction between A-POSS and PET i.e. amide bond formation was characterized by XPS (**Fig. 1b.**). The carbon (C) 1s XPS spectrum of PET showed four distinctive peaks. The main peak at ~284.7 eV is assigned to the C-C/C-H of terephthalate rings, the peak at ~286.4 eV assigned to the -**C**H_2-O of ester, the peak at ~288.6 eV is assigned to -(**C**=O)-O of

ester and carboxylic acid, and the weak peak at ~291.1 eV is due to the π-π* shake-up transition of terephthalate rings [18, 19]. The C 1s XPS spectrum of A05 shows the decreased peak at ~288.6 eV compared to that of PET probably due to the chemical conjugation between the carboxylic acid of PET and the amine of A-POSS. The nitrogen (N) spectrum of A-POSS gives a sharp and narrow peak that is a sign of R-**N**-H_2 (amine) [16, 18]. The amine peak in the N spectrum of A05 was broader than that of PET and shifted to lower energy level probably due to the formation of R-**N**H-(C=O) [19].

Table. 1. Sample list of PET and PET/T_{12} POSS composites.

Fig. 1. Schematic illustration of (a) non-reactive, (b) amine-functionalized T_{12} POSS (A-POSS), and (c) conjugation reaction between PET and A-POSS. (d) XPS C 1s spectra of PET and A05 composite. (e) XPS N 1s spectra of A-POSS and A05 composite.

Moreover, the T_{12} POSS dispersibility in PET was evaluated by the cross-sectional silicon (Si) FE-EPMA mapping images (**Fig. 2.**). While the A-POSS nanoparticles were well-dispersed in the A05 composite, 5-10 μm sized N-POSS aggregates were observed in the N05 composites. These results suggest that A-POSS gives higher dispersibility in PET than N-POSS due to the amide conjugation reaction [20].

Fig. 2. FE-EPMA Si mapping images of PET/T_{12} POSS composites: (a) A05 and (b) N05.

Also, these results are supported by wide angle X-ray scattering (WAXS) patterns (**Fig. S2.**). The WAXS pattern of N10 shows prominent peaks at around $2\theta=8^o$, which are found not in the pattern of pristine PET but in the patterns of N-POSS and A-POSS. However, the pattern of A10 shows almost negligible peaks at around $2\theta=8^o$. The results imply that A-POSS possibly has higher dispersibility with

PET matrix than N-POSS [12, 13]. Meanwhile, the other all peaks of both A-POSS and N-POSS composites with the range of 10 to 50º correspond with those of pristine PET, suggesting that the two different T_{12} POSS do not affect PET crystal structure.

3.2. Thermal properties of PET composites

The effects of the chemically conjugated A-POSS on the thermal properties of PET were investigated by DSC (**Fig. 3. And Fig. S3.**). The crystallization temperature and heat of crystallization of PET and PET composites were obtained during the cooling trace (**Fig. 3a, b.**). Pristine PET has a crystallization temperature of approximately 141 °C. As shown, the effects of N-POSS and A-POSS incorporation increased the crystallization temperature of PET up to ~165 and ~176 °C, respectively. These results suggest that T_{12} POSS plays a role of nucleating agent and the chemically conjugated A-POSS forms more well-dispersed nuclei in the PET matrix. Moreover, our T_{12} POSS was more effective as nucleating agent for PET than T_8 POSS, which shows an approximate 5 °C fall or 6-23 °C rise in the crystallization temperature [12, 13, 21]. This was attributed to the fact that T_{12} POSS particles are more poorly packed with each other than T_8 POSS particles because T_{12} POSS particles have lower symmetry T_8 POSS particles [22, 23]. Therefore T_{12} POSS gives greater interfacial area with PET where heterogonous nucleation occurs. In addition, the heat of crystallization data showed a similar tendency with the crystallization temperature, as T_{12} POSS-induced nuclei increased the crystallinity of PET.

The T_g and onset melting temperature of PET composites were obtained during the second heating trace (**Fig. 3c, d.**). T_g increases with the content of T_{12} POSS because the inorganic nanoparticles restrict the molecular motion of PET chain ends. The A-POSS composites showed higher T_g values over the N-POSS composites due to the relatively more homogeneous dispersion of the A-POSS particles. Onset melting temperature decreases with the content and the dispersibility of T_{12} POSS probably because of the decreased crystal size [13, 21].

Fig. 3. (a) Crystallization temperature and (b) heat of crystallization of A-POSS and N-POSS PET composites during the cooling trace. (c) Glass transition temperature (T_g) and (d) onset melting temperature of A-POSS and N-POSS PET composites during the second heating trace. The data were obtained using a differential scanning calorimetry (DSC). The data of triple samples represent mean ± standard deviation.

3.3. Dynamic crystallization rate of PET composites

To evaluate the effects of the chemically conjugated A-POSS on the crystallization rate of PET within a melt spinning process and an injection process, the shear-induced crystallization time of the PET composites were measured by dynamic rheological measurements. The samples were fully melted at 280 °C, then time sweep measurements were conducted over the angular frequency (ω) of 0.5 at 220 °C under inert nitrogen atmosphere. In the general G'-time plot of PET composites, the G' gradually increases with time and saturates when the crystallization reaches an equilibrium (**Fig. 4a.**) [21]. The shear-induced crystallization time was determined by the time difference between the abrupt G' increase and the level-off point. The addition of T_{12} POSS decreases the shear-induced crystallization time up to ~34% of that of pristine PET, supporting the notion that T_{12} POSS is a more effective nucleating agent for PET than T_8 POSS which decreases the shear-induced crystallization time up to ~60% of that of pristine PET [21]. The A-POSS composites have shorter shear-induced crystallization time than the N-POSS composites. The shear-induced crystallization time of the A-POSS composite reaches saturation at <0.5 wt. %, while that of the N-POSS composites gradually decreases with the T_{12} POSS content in the examine region (**Fig. 4b.**). These results are probably because the well-dispersed A-POSS induces a higher number of the collisions between the nuclei and the polymer chain [24]. Thus, the addition of A-POSS may effectively reduce the post-shrinkage of PET products and the retardation of PET molding process over N-POSS.

Fig. 4. (a) Dynamic storage modulus (G') versus time of PET composite melts over the angular frequency (ω) of 0.5 at 220 °C. (b) Shear-induced crystallization time (or dynamic crystallization time) of PET composites at 220 °C. The data of triple samples represent mean ± standard deviation with statistical significance [* $p < 0.05$, not significant (NS) $p > 0.05$; unpaired t-test).

3.4. Tensile properties of PET composites

To evaluate the effects of the chemically conjugated A-POSS on the mechanical properties of PET, the tensile properties of the PET composites were measured (**Table 2**). It was found that the addition of T_{12} POSS increases the Young's modulus and tensile strength due to the increased crystallinity. Moreover, the A-POSS composites showed higher Young's moduli and tensile strength values than the N-POSS composites because of the higher crystallinity induced nucleating effect.

Table. 2. Tensile mechanical properties of PET, A15, and N15. The data of triple samples represent mean ± standard deviation.

3.5. Rheological properties of PET composite melts

To evaluate the melt processing stability of the PET composites, the rheological properties of PET and their composites with T_{12} POSS were examined at 280 °C. The dynamic viscosity (η')-angular frequency (ω) plots of the melted PET, A15, and N15 are presented in **Fig. 5a**. While the A15 shows a more comparable η' pattern with pristine PET in the examined ω range, the N15 shows the higher η' pattern than the pristine PET in the low ω range. It suggests that the aggregation of N-POSS particles interrupts the smooth flow of PET melt [21, 25]. The linear master curve of G' versus loss modulus (G") logarithmic plots i.e. Cole-Cole plot indicates a homogeneous and isotropic polymer melt (**Fig. 5b.**) [21, 25]. The Cole-Cole plot of A15 gives relatively less scattering of data points to that of PET, while the plot of N15 gives the notable deviation of data points and data slopes compared with that of PET. The tendency of the η' and Cole-Cole plots suggests that the A-POSS particles has little effect on the

homogeneity of the system probably due to the low degree of aggregation. However, the incorporation N-POSS into PET gives a considerable increase in the degree of heterogeneity of the PET melt system due to the aggregation of N-POSS. It suggests that the chemical conjugation between PET and POSS could improve the melt processing stability of PET/POSS composites [26].

Fig. 5. (a) The complex viscosity (η') versus angular frequency (ω) plots of PET composite melts at 280 ^{o}C. (b) The linear master curve of storage modulus (G') versus loss modulus (G") logarithmic plots.

4. Conclusions

An aminopropyl functionalized T_{12} POSS (A-POSS) has been studied as a nucleating agent for PET in comparison with a type of non-functional fully phenyl-substituted T_{12} POSS (N-POSS) and previously reported T_8 POSS. The aminopropyl groups of A-POSS allowed for chemically conjugation to the PET chains, giving a more homogeneous dispersion in PET matrix than that of N-POSS. Moreover, the addition of A-POSS functioned to increase crystallization temperature and the shear-induced crystallization rate of PET than N-POSS and previously reported T_8 POSS. In addition, A-POSS improved the thermal and tensile properties of PET in terms of T_g, Young's modulus, and tensile strength. Rheological studies revealed that the A-POSS has less effect on the homogeneity of PET melt within melt processes than non-functional T_{12} POSS due to the reduced particle aggregation.

Acknowledgement

This work was financially supported by the Technology Innovation Program (10070150) funded By the Ministry of Trade, Industry & Energy (MOTIE, Korea), and partially supported by a grant from Research Center for Chemical Biotechnology of Korea Research Institute of Chemical Technology (SI 1709).

ACCEPTED MANUSCRIPT

References

(1) D. W. Chae, B. C. Kim, Thermal and rheological properties of highly concentrated PET composites with ferrite nanoparticles, Comp. Sci. Technol. 67 (2007) 1348-1352.

(2) K. A. Anand, U. S. Agarwal, R. Joseph, Carbon nanotubes induced crystallization of poly(ethylene terephthalate), Polymer. 47 (2006) 3976-3980.

(3) H. Matsuda, T. Asakura, B. Nagasaka, K. Sato, Relationship between sequence distribution and thermal properties of the transesterification product between poly(ethylene terephthalate) and poly(butylene terephthalate), Macromolecules. 37 (2004) 4651-4657.

(4) G. Aravinthan, D. D. Kale, Blends of poly(ethylene terephthalate) and poly(butylene terephthalate), J. Appl. Polymn. Sci. 98 (2005) 75-82

(5) C. I. W. Calcagno, C. M. Mariani, S. R. Teixeira, R. S. Mauler, The effect of organic modifier of the clay on morphology and crystallization properties of PET nanocomposites, Polymer. 48 (2007) 966-974.

(6) D. W. Litchfield, D. G. Baird, The role of nanoclay in the generation of poly(ethylene terephthalate) fibers with improved modulus and tenacity, Polymer. 49 (2008) 5027-5036.

(7) H. J. Yoo, K. H. Kim, S. K. Yadav, J. W. Cho, Effects of carbon nanotube functionalization and annealing on crystallization and mechanical properties of melt-spun carbon nanotubes/poly(ethylene terephthalate) fibers, Comp. Sci. Technol. 72 (2012) 1834-1840.

(8) W. Liu, X. Tian, P. Cui, Y. Li, K. Zheng, Y. Yang, Preparation and characterization of PET/silica nanocomposites, J. Appl. Poly. Sci. 91 (2004) 1229-1232.

(9) S. H. Phillips, T. S. Haddad, S. J. Tomczak, Developments in nanoscience: polyhedral oligomeric silsesquioxane (POSS)-polymers, Curr. Opin. Solid State Mater. Sci. 8 (2004) 21-29.

(10) N. C. Escudé, E. Y. –X. Chen, Stereoregular methacrylate-POSS hybrid polymers: syntheses and nanostructured assemblies, Chem. Mater. 21 (2009) 5743-5753.

(11) A. S. Lee, S. S. Choi, S. Y. Oh, H. S. Lee, B. Kim, S. S. Hwang, K. Y. Baek, Incompletely condensed POSS-based spin-on-glass networks for impeccable ultra low-*k* integration, J. Mater. Chem. C. 3 (2015) 11605-11611.

(12) F. C. L. Ciolacu, N. R. Choudhury, N. Dutta, E. Kosior, Molecular level stabilization of poly(ethylene terephthalate) with nanostructured open cage trisilanolisobutyl-POSS, Macromolecules. 40 (2007) 265-272.

(13) H. –U. Kim, Y. H. Bang, S. M. Choi, K. H. Yoon, Morphology and mechanical properties of PET by incorporation of amine-polyhedral oligomeric silsesquioxane, Comp. Sci. Technol. 68 (2008) 2739-2747.

(14) K. H. Yoon, M. B. Polk, J. H. Park, B. G. Min, D. A. Schiraldi, Properties of poly(ethylene terephthalate) containing epoxy-functionalized polyhedral oligomeric silsesquioxane, Polym. Int. 54 (2005) 47-53.

(15) A. S. Lee, S. –S. Choi, H. S. Lee, K. Y. Baek, S. S. Hwang, S. S, A new, higher yielding synthetic route towards dodecaphenyl cage silsesquioxanes: synthesis and mechanistic insights, Dalton Trans. 41 (2012) 10585-10588.

(16) S. –S. Choi, A. S. Lee, S. S. Hwang, K. Y. Baek, Structural control of fully condensed polysilsesquioxanes: ladderlike vs cage structured polyphenylsilsesquioxanes, Macromolecules. 48 (2015) 6063-6070.

(17) G. Li, L. Wang, H. Ni, C. U. Pittman Jr., Polyhedral oligomeric silsesquioxane (POSS) polymers and copolymers: A review, J. Inorg. Organomet. Polym. 11 (2011) 123-154.

(18) A. Singh, Z. Salmi, N. Joshi, P. Jha, A. Kumar, H. Lecoq, S. Lau, M. M. Chehimi, D. K. Aswal, S. K. Gupta, Photo-induced synthesis of polypyrrole-silver nanocomposite films on N-(3-trimethoxysilylpropyl)pyrrole-modified biaxially oriented polyethylene terephthalate flexible substrates, RSC Adv. 3 (2013) 5506-5523.

(19) K. H. Hong, K. W. Oh, T. J. Kang, Polyaniline–nylon 6 composite fabric for ammonia gas sensor, J. Appl. Polym. Sci. 92 (2004) 37-42.

(20) Y. M. Ha, T. Amna, M. H. Kim, H. C. Hassan, M. S. Khil, Novel silicificated PVAc/POSS composite nanofibrous mat via facile electrospinning technique: Potential scaffold for hard tissue engineering, Colloids Surf. B. 102 (2013) 795-802.

(21) S. J. Lee, W. G. Hahm, T. Kikitani, B. C. Kim, Effects of clay and POSS nanoparticles on the quiescent and shear-induced crystallization behavior of high molecular weight poly(ethylene terephthalate), Polym. Eng. Sci. 49 (2009) 317-323.

(22) V. Ervithayasuporn, S. Chimjarn, Synthesis and isolation of methacrylate- and acrylate-functionalized polyhedral oligomeric silsesquioxanes (T_8, T_{10}, and T_{12}) and characterization of the relationship between their chemical structures and physical properties, Inorg. Chem. 52 (2013) 13108-13112.

(23) J. C. Furgal, J. H. Jung, T. Goodson III, R. M. Laine, Analyzing structure-photophysical property relationships for isolated T_8, T_{10}, and T_{12} stilbenevinylsilsesquioxanes, J. Am. Chem. Soc. 135 (2013) 12259-12269.

(24) S. –I. Han, J. S. Lim, D. K. Kim, M. N. Kim, S. S. Im, *In situ* polymerized poly(butylene succinate)/silica nanocomposites: Physical properties and biodegradation, Polym. Degrad. Stab. 93 (2008) 889-895.

ACCEPTED MANUSCRIPT

(25) E. S. Kim, B. C. Kim, S. H. Kim, Structural effect of linear and star-shaped poly(L-lactic acid) on physical properties, J. Polym. Sci. Part B: Polym. Phy. 42 (2004) 939-946.

(26) Y. P. Jeon, C. L. Cox, Modeling of multifilament PET fiber melt-spinning, J Appl. Polym. Sci. 110 (2008) 2153-2163.

ACCEPTED MANUSCRIPT

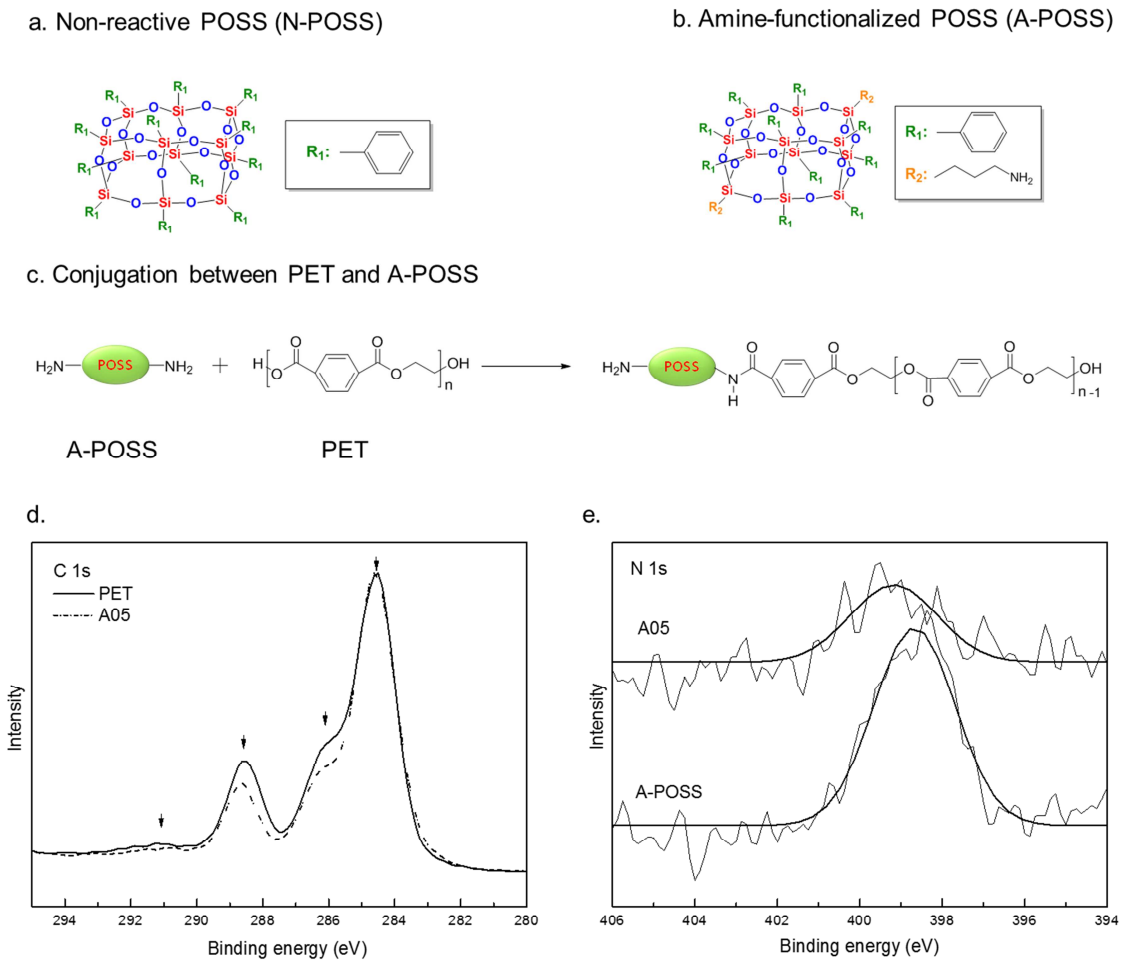

Fig. 1. Schematic illustration of (a) non-reactive, (b) amine-functionalized T_{12} POSS (A-POSS), and (c) conjugation reaction between PET and A-POSS. (d) XPS C 1s spectra of PET and A05 composite. (e) XPS N 1s spectra of A-POSS and A05 composite.

ACCEPTED

ACCEPTED MANUSCRIPT

Table 1. Sample list of PET and PET/T_{12} POSS composites.

Code name	PET wt. %	A-POSS wt. %	N-POSS wt. %
PET	100	0	0
A05	99.5	0.5	0
A10	99	1	0
A15	98.5	1.5	0
N05	99.5	0	0.5
N10	99	0	1
N15	98.5	0	1.5

ACCEPTED MANUSCRIPT

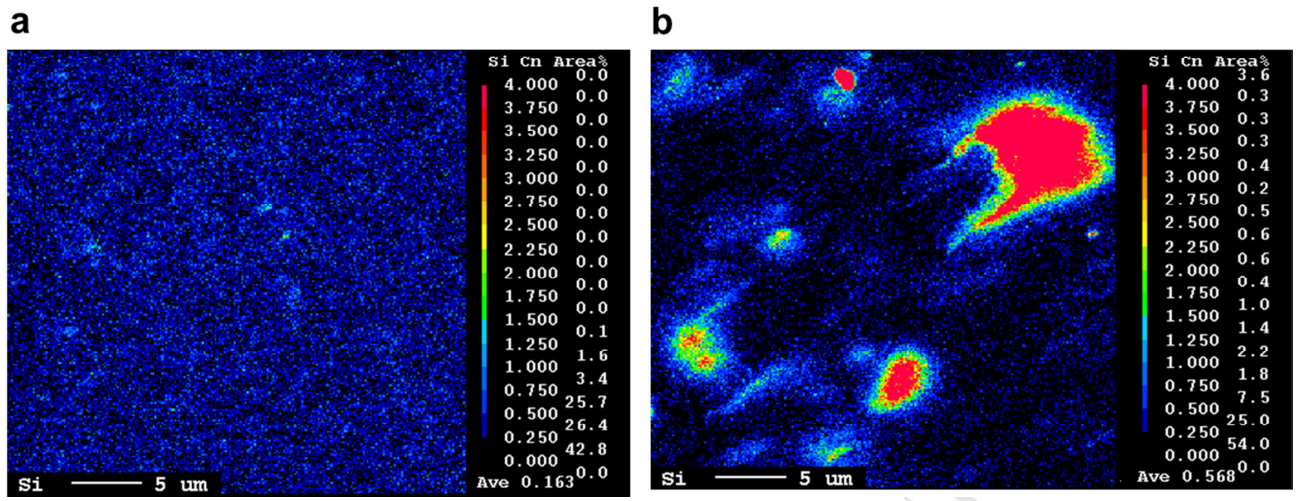

Fig. 2. FE-EPMA Si mapping images of PET/T_{12} POSS composites: (a) A05 and (b) N05.

ACCEPTED MANUSCRIPT

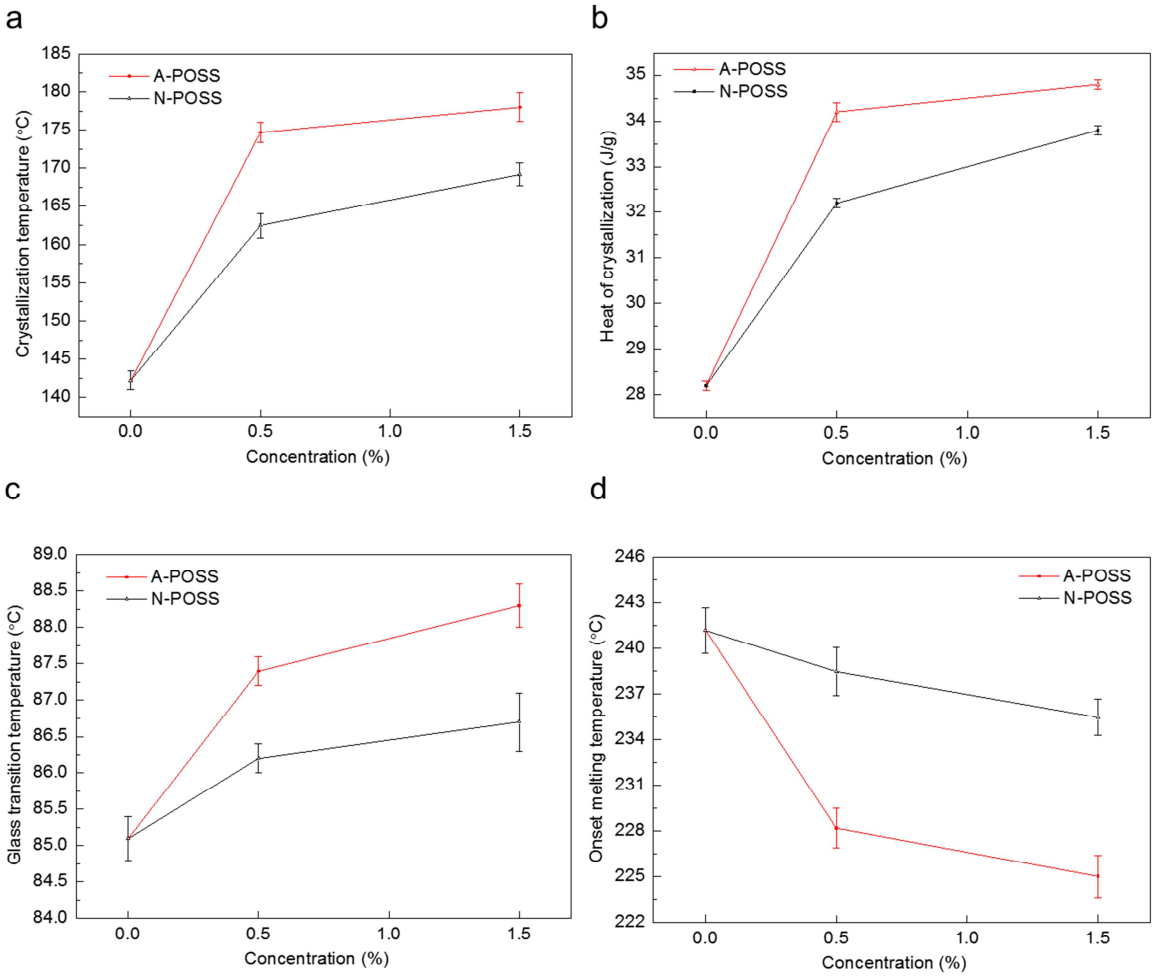

Fig. 3. (a) Crystallization temperature and (b) heat of crystallization of A-POSS and N-POSS PET composites during the cooling trace. (c) Glass transition temperature (T_g) and (d) onset melting temperature of A-POSS and N-POSS PET composites during the second heating trace. The data were obtained using a differential scanning calorimetry (DSC). The data of triple samples represent mean ± standard deviation.

ACCEPTED

ACCEPTED MANUSCRIPT

Code name	Young's modulus (GPa)	Tensile strength (MPa)
PET	2.2 ± 0.1	92.1 ± 2.1
A15	2.9 ± 0.2	109.9 ± 1.6
N15	2.4 ± 0.1	101.3 ± 2.2

Table 2. Tensile mechanical properties of PET, A15, and N15. The data of triple samples represent mean ± standard deviation.

ACCEPTED MANUSCRIPT

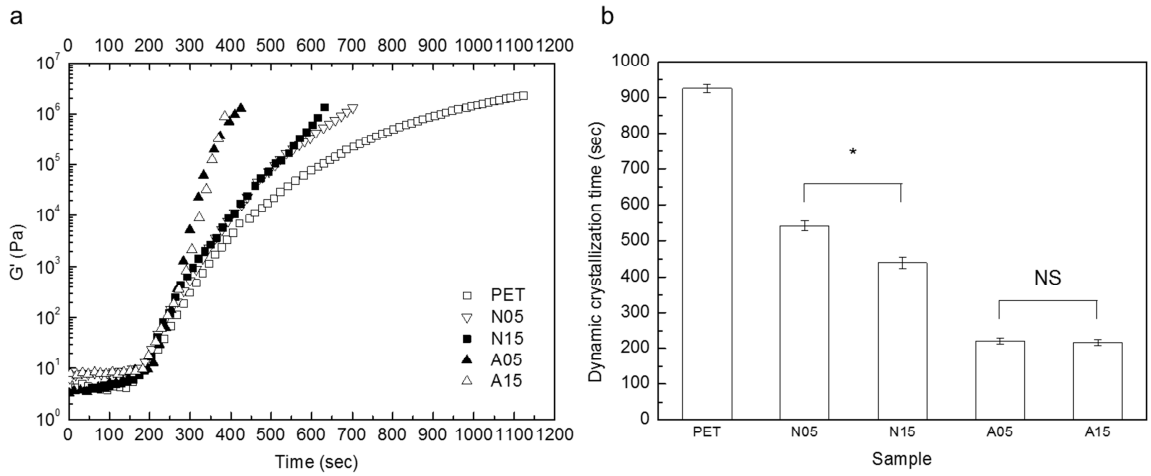

Fig. 4. (a) Dynamic storage modulus (G') versus time of PET composite melts over the angular frequency (ω) of 0.5 at 220°C. (b) Shear-induced crystallization time (or dynamic crystallization time) of PET composites at 220 °C. The data of triple samples represent mean ± standard deviation with statistical significance [* $p < 0.05$, not significant (NS) $p > 0.05$; unpaired t-test).

ACCEPTED MANUSCRIPT

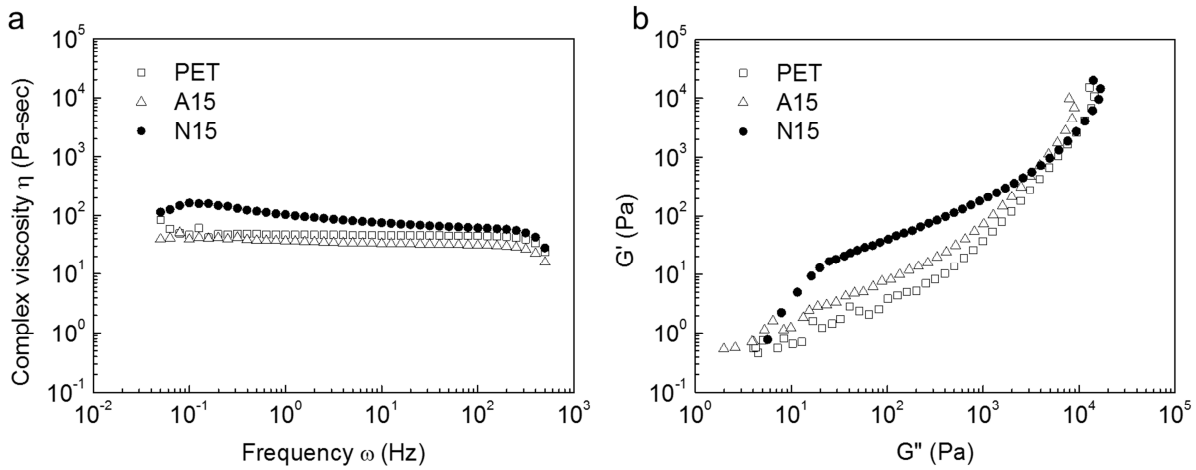

Fig. 5. (a) The complex viscosity (η') versus angular frequency (ω) plots of PET composite melts at 280 ^{o}C. (b) The linear master curve of storage modulus (G') versus loss modulus (G") logarithmic plots.

ACCEPTED MANUSCRIPT